International Journal of Cardiology 281 (2019) 8–14

Contents lists available at ScienceDirect

International Journal of Cardiology

journal homepage: www.elsevier.com/locate/ijcard

Myocardial viability of the peri-infarct region measured by T1 mapping post manganese-enhanced MRI correlates with LV dysfunction

Yuko Tada, Shahriar Heidary, Atsushi Tachibana, Junaid Zaman, Evgenios Neofytou, Rajesh Dash, Joseph C. Wu, Phillip C. Yang *

Department of Medicine (Cardiovascular Medicine) and Cardiovascular Institute, Stanford University School of Medicine, Stanford, CA, United States of America

ARTICLE INFO

Article history:
Received 28 September 2018
Received in revised form 21 January 2019
Accepted 29 January 2019
Available online 31 January 2019

Keywords:
Manganese-enhanced MRI
T1 mapping
Myocardial viability
Myocardial infarction

ABSTRACT

Background: Manganese-enhanced MRI (MEMRI) detects viable cardiomyocytes based on the intracellular manganese uptake via L-type calcium-channels. This study aimed to quantify myocardial viability based on manganese uptake by viable myocardium in the infarct core (IC), peri-infarct region (PIR) and remote myocardium (RM) using T1 mapping before and after MEMRI and assess their association with cardiac function and arrhythmogenesis.

Methods: Fifteen female swine had a 60-minute balloon ischemia-reperfusion injury in the LAD. MRI (Signa 3T, GE Healthcare) and electrophysiological study (EPS) were performed 4 weeks later. MEMRI and delayed gadolinium-enhanced MRI (DEMRI) were acquired on LV short axis. The DEMRI positive total infarct area was subdivided into the regions of MEMRI-negative non-viable IC and MEMRI-positive viable PIR. T1 mapping was performed to evaluate native T1, post-MEMRI T1, and delta R1 ($R1_{post}$-$R1_{pre}$, where R1 equals 1/T1) of each territory. Their correlation with LV function and EPS data was assessed.

Results: PIR was characterized by intermediate native T1 (1530.5 ± 75.2 ms) compared to IC (1634.7 ± 88.4 ms, $p = 0.001$) and RM (1406.4 ± 37.9 ms, $p < 0.0001$). Lower post-MEMRI T1 of PIR (1136.3 ± 99.6 ms) than IC (1262.6 ± 126.8 ms, $p = 0.005$) and higher delta R1 (0.23 ± 0.08 s^{-1}) of PIR than IC (0.18 ± 0.09 s^{-1}, $p = 0.04$) indicated higher myocardial manganese uptake of PIR compared to IC. Post-MEMRI T1 ($r = -0.57$, $p = 0.02$) and delta R1 ($r = 0.51$, $p = 0.04$) of PIR correlated significantly with LVEF.

Conclusions: PIR is characterized by higher manganese uptake compared to the infarct core. In the subacute phase post-IR, PIR viability measured by post-MEMRI T1 correlates with cardiac function.

1. Introduction

Total myocardial infarct size detected by delayed gadolinium enhancement MRI (DEMRI) is an established prognostic marker; however, the relative importance of the peri-infarct region (PIR) adjacent to the non-viable infarct core (IC) has been noted recently [1–4]. Up to 10% of DEMRI positive myocardial infarct consists of histologically viable PIR, with reduced signal of the gadolinium-based contrast agent [5–8]. The PIR, featured by histological tissue heterogeneity, represents a key therapeutic target for revascularization or novel biologics as it undergoes active reparative and remodeling processes [9–13]. The presence of PIR has been reported as an independent predictor of ventricular arrhythmia, remodeling and mortality [2,10,11,14,15]. Hence, there is clear diagnostic value to characterize the PIR in vivo.

Recent advances in T1 mapping technique could help characterize the PIR more precisely and identify its pathological relevance. Although expansion of the extracellular volume (ECV) fraction impacts clinical outcomes [16–18], one of the intrinsic disadvantages is ECV does not detect the dysfunctional myocardium directly. In contrast, manganese enhanced MRI (MEMRI) detects viable cardiomyocytes through their ability to take up manganese ions through the L-type calcium channels [19,20]. PIR can be delineated by the dual MEMRI and DEMRI contrast in which MEMRI positive viable cardiomyocytes are located inside DEMRI positive myocardial scar [21,22]. The PIR delineated by this method has been characterized by transmission electron microscopy (TEM), revealing the injured cellular architecture and contractile components of the cardiomyocytes [21]. Because of the rapid first pass uptake of manganese by cardiomyocytes, short plasma half-life, and long intracellular

Abbreviations: PIR, peri-infarct region; IC, infarct core; MEMRI, manganese-enhanced MRI; EPS, electrophysiological study; DEMRI, delayed gadolinium-enhanced MRI; RM, remote myocardium; MI, myocardial infarction; ECV, extracellular volume; IR, ischemia-reperfusion; LVEDV, LV end-diastolic volume; LVESV, LV end-systolic volume; LVM, LV mass; BSA, body surface area; LVEDVI, LVEDV index; LVESVI, LVESV index; ROI, region of interest; SI, signal intensity; TI, total infarct; AAR, area at risk; TTC, 2,3,5-triphenyltetrazolium chloride stain.

* Corresponding author at: Stanford University School of Medicine, 269 Campus Drive, CCSR 3115C, Stanford, CA 94305, United States of America.
E-mail address: phillip@stanford.edu (P.C. Yang).

https://doi.org/10.1016/j.ijcard.2019.01.101
0167-5273/

retention period, the R1 (i.e. 1/T1) change in each voxel before and after MEMRI could be a unique marker of myocardial viability [23–25]. Thus, myocardial injury in the heterogeneous infarct zones can be assessed based on the differential myocardial manganese uptake using T1 mapping before and after MEMRI. This MEMRI viability signal may indicate LV remodeling and arrhythmogenic potential more strongly when compared to the assessment of necrosis or fibrosis by native T1 or ECV mapping.

This study aimed to quantify the variable myocardial viability signals of IC, PIR and RM using T1 mapping before and after MEMRI in swine in the subacute phase at 4 weeks after the induction of ischemia-reperfusion (IR) injury and assess their association with cardiac function and arrhythmogenesis.

2. Materials and methods

2.1. Swine ischemia-reperfusion (IR) injury model

The animal protocol was approved by the Stanford University Administrative Panel on Laboratory Animal Care. An ischemia-reperfusion (IR) model was created in 15 female swine (Yorkshire or Yucatan, juvenile (<1 year old), 30–57 kg, Pork Power (Turlock, California)) as described previously [21]. The swine were anesthetized by inhaled isoflurane (1–3%). A 10-mm over-the-wire angioplasty balloon was placed in the proximal left anterior descending coronary artery (LAD) at the first diagonal branch and inflated for 60 min. The reperfusion was confirmed by coronary angiography. Amiodarone 150 mg IV bolus was prophylactically administered 20 min after the start of balloon occlusion. If indicated, non-synchronized direct current defibrillation was performed at 360 J. Swine which did not undergo IR injury underwent MRI to obtain normal control data ($n = 4$).

2.2. MRI study

Cardiac MRI was performed (Signa HDx 3.0T; GE Healthcare), using an 8-channel chest coil 4 weeks after the IR induction. Swine were anesthetized using 1.0–3.0% isoflurane. MRI was acquired with ECG gating and breath-holding. The cine, MEMRI, and DEMRI were acquired as described previously [21]. Briefly, cine images were acquired using steady state free procession (TR 3.4 ms; TE min-full; flip angle 45°; thickness 8 mm; matrix 224 × 224; and field of view [FOV] 28 cm). MEMRI was obtained using fast gradient echo-inversion recovery (FGRE-IR) sequence (TR 6.2 ms; TE 2.9 ms; flip angle 15°; thickness 8 mm; matrix 224 × 192; FOV 28 cm; TI 300–600 ms) 25–40 min after IV infusion of EVP1001-1 at 20.3 μmol/kg (2.0 μmol/kg/min) (Eagle Vision Pharmaceutical Corp; Downington, PA). EVP 1001-1 contains free manganese in a readily available form [23]. After a 30-minute washout period, 0.2 mmol/kg of Gd-DTPA (Magnevist, Bayer Health Care Pharma AG, Berlin, Germany) was administered. DEMRI was obtained using FGRE-IR sequence (TI 250–300 ms) 10–25 min later. Saturation recovery T1 mapping was performed before (native T1) and after MEMRI (post-MEMRI T1) using SMRAT1Map sequence (GE Healthcare, WI); non-selective IR; flip angle 50°; matrix 192 × 128; FOV 28 cm; TI 100 ms; thickness 8 mm; 3 inversions; TI increment 100–150 ms, end-diastolic phase) at mid LV short axis to include both the infarct and non-infarct [26].

2.3. MRI analysis

Cine MRI was analyzed using AZE VirtualPlace™ (Tokyo, Japan) to determine LV end-diastolic volume (LVEDV), LV end-systolic volume (LVESV), LVEF, and LV muscular volume. LV mass (LVM) was determined as LV muscular volume × 1.05 g/cm^3. Body surface area (BSA) (m^2) was determined as 0.0734 × body weight (kg)^(0.652) to calculate indexed values of LVEDV (LVEDVI), LVESV (LVESVI), and LVM (LVMI) [27].

MEMRI, DEMRI, and T1 mapping were analyzed using the software created in Matlab (Mathworks, Natick, MA). First, epicardial and subendocardial contours were traced manually on the short axis images. Areas with MEMRI defect, infarct core (IC) and DEMRI enhancement total infarct (TI) were semi-automatically traced by the standard deviation (SD) method. A region of interest (ROI) in RM was placed on the septum or lateral wall sufficiently apart from the infarct. After multiple SDs (2–6 SDs) were tested, 4SD, which corresponded best with the visual assessment of the infarct signals, was adopted as the threshold for both MEMRI and DEMRI by consensus analysis of three reviewers. As the TI size is larger than the IC in this IR injury model, PIR size was calculated by subtracting IC from TI (Fig. 1) [21,22]. Infarct size was determined as %LV and mass (g) determined by multiplication by LVM.

MEMRI, DEMRI and T1 mapping images, obtained at the same mid-LV location, were used to analyze the T1 values. MEMRI and DEMRI images were merged on the computer to subdivide DEMRI positive total infarct (TI) into MEMRI negative nonviable IC and MEMRI positive viable PIR (Fig. 1). The TI, IC, PIR, and RM areas were delineated on the pre and post-MEMRI T1 mapping, obtained at the same location, to calculate the T1 values of each region (Fig. 1). Manganese uptake in each territory was quantified as R1 change of the ROI denoted as delta R1 = R1 (post-MEMRI) − R1 (pre-MEMRI), where R1 = 1/T1. The mean T1 values and delta T1 were calculated and correlations between T1 or delta R1 and LVEF data were examined. Swine were divided into the higher EF group (EF ≥ median) and lower EF group (EF < median) to compare T1 and delta R1 between the 2 groups.

2.4. Electrophysiology study (EPS)

After MRI study, 10 swine underwent electrophysiology study (EPS) for arrhythmia inducibility. Electrode catheters were placed in the His bundle and in the RV apex or outflow tract. Using constant-current/voltage programmable stimulator (Harvard Instruments HA-HSE Stimulator C, model 733716), programmed extra stimulation with up to 3 extra-stimuli at S1 drive train cycle lengths of 600, 500, and 400 ms was performed. We also used burst ventricular pacing of 5 to 15 ventricular stimuli at cycle lengths of 350 to 150 ms. If VT, ventricular refractory state, VF, or polymorphic VT was induced, the pacing protocol was stopped. We calculated the difference between the baseline drive train and extra-stimulus or burst pacing interval to induce LV arrhythmia (baseline-S2 interval) as a marker of arrhythmogenesis.

2.5. Staining of the area at risk and infarct core

After MRI and EPS studies were done, swine had an injection of 1% Evans blue dye and 2,3,5-triphenyltetrazolium chloride stain (TTC) to delineate the area at risk (AAR) and the infarct core, as described previously [21]. Under anesthesia, guiding catheters were inserted into both the right and left coronary arteries. The LAD was occluded with an over-the-wire catheter at the same location of the previous occlusion. During the balloon occlusion of the LAD, 1% Evans blue dye was injected into the left (60 ml) and right (30 ml) coronary arteries to delineate Evans blue negative area at risk (AAR) and Evans blue positive perfused (normal) myocardium. In addition, 20 to 30 ml of 1% TTC solution was injected through the guidewire lumen of the over-the-wire balloon catheter,

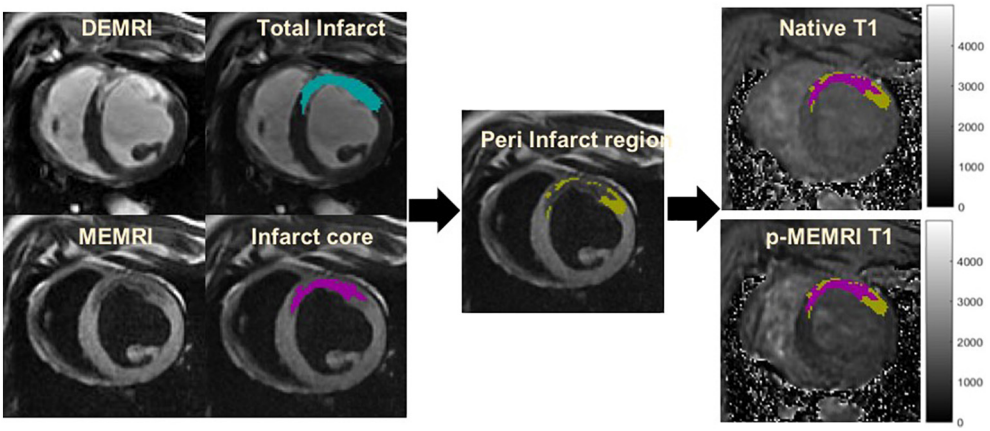

Fig. 1. Delineation of total infarct, core infarct, and peri-infarct region (PIR). Areas with DEMRI positive total injury (*aqua*) were divided into non-viable MEMRI negative infarct core (*magenta*) and viable MEMRI positive PIR territories (*yellow*). Representative native and post-MEMRI T1 maps obtained with SMART1Map sequence are shown. Infarct core, peri-infarct, and total infarct areas were superimposed on each map to obtain average T1 value in each territory. In this example, infarct core (*magenta*) and PIR (*yellow*) are depicted on the native T1 and post-MEMRI T1 maps. Delta R1 was calculated from native and post-MEMRI T1 values of each ROI.

which stains viable myocardium containing mitochondrial dehydrogenase enzymes red and leaves non-viable myocardium white (infarct core). Finally, the pig was euthanized with an intravenous potassium chloride injection. The excised heart was cut in 1 cm-thick cross sectional slices and fixed with 10% formalin. The slices were cut into pieces containing IC, PIR, and RM, respectively and embedded in paraffin. The sliced sections were stained with hematoxylin eosin (H&E) for morphological observation.

2.6. Statistical analysis

All data were expressed as mean ± SD. Median, 1st, and 3rd quartile values were determined. Mean values among more than two groups were compared using one-way ANOVA. Mean values between two groups were compared using a two-tail *t*-test for normal distribution and non-parametric analysis for data without normal distribution. Differences with values of $p < 0.05$ were considered significant. Pearson's correlation coefficient (r) was determined to test linear correlation between two sample sets.

3. Results

3.1. Tissue characterization of infarct core (IC) and peri-infarct region (PIR)

DEMRI-MEMRI discriminated the total infarct (TI), IC, and PIR of 15 swine, which were 30.2 ± 6.2%, 21.8 ± 5.6%, and 8.4 ± 5.9% of total LV mass, respectively. The mean LVEF, LVEDV, and LVM were 27.9 ± 8.7%, 78.8 ± 15.5 ml (LVEDVI 94.3 ± 25.0 ml/m^2), and 65.7 ± 10.9 g (LVMI 78.8 ± 15.5 ml/m^2). The LVEF, LVEDV, and LVM of the control swine were 60.1 ± 8.0%*, 49.7 ± 10.3 ml* (LVEDVI 60.5 ± 4.6 ml/m^{2*}), and 52.4 ± 3.5 g* (LVMI 65.1 ± 9.6 g/m^2), respectively (*significantly higher or lower compared to the IR group). The IC, PIR, and RM were characterized by measurement of native T1, post-MEMRI T1, and delta R1, which demonstrated distinct values of each region (Table 1, Supplementary Fig. 1). PIR had significantly increased native T1 (1530.5 ± 75.2 ms) compared to RM (1406.4 ± 37.9 ms, $p < 0.0001$, Table 1, Supplementary Fig. 1) and decreased native T1 compared to IC (1634.7 ± 88.4 ms, $p = 0.001$). Post-MEMRI T1 in PIR (1136.3 ± 99.6 ms) was significantly lower than IC (1262.6 ± 126.8 ms, $p = 0.005$) and higher than RM (956.7 ± 138.1 ms, $p = 0.0001$). Delta R1 of PIR (0.23 ± 0.08 s^{-1}) suggested higher myocardial manganese uptake compared to IC (0.18 ± 0.09 s^{-1}, $p = 0.04$) and lower manganese uptake than RM (0.35 ± 0.19 s^{-1}, $p = 0.01$).

Native and post-MEMRI T1 and delta R1 of RM were comparable to those of the normal myocardium (septum and lateral walls) of the control swine (Table 1). No significant correlation was found between native T1 and post-MEMRI T1 values of each region. Heart rate at the timing of manganese injection had no significant correlation with the myocardial native T1, post-MEMRI T1, or delta R1.

3.2. MEMRI and LV function

A negative correlation between LVEF and the %total infarct (TI) was confirmed ($r = -0.71$, $p = 0.001$) while %IC ($r = -0.36$, $p = 0.18$) or % PIR size ($r = -0.40$, $p = 0.14$) did not correlate with LVEF significantly. Similarly, %TI correlated with LVEDV ($r = 0.60$, $p = 0.01$) and LVEDVI ($r = 0.57$, $p = 0.02$). However, %IC or %PIR did not correlate with LVEDV or LVEDVI.

The relationships between LV function and native T1, post-MEMRI T1, and delta R1 of TI, IC, PIR, and RM were examined. Post-MEMRI T1 of PIR ($r = -0.57$, $p = 0.02$) had a clear negative correlation with LVEF while post-MEMRI T1 of IC ($r = -0.53$, $p = 0.04$) also had a weaker but significant correlation (Fig. 2). Post-MEMRI T1 of PIR also correlated with LVEDV ($r = 0.54$, $p = 0.03$) and LVEDVI ($r = 0.53$, $p = 0.03$). Similarly, delta R1 of PIR showed significant correlation of myocardial manganese uptake with LVEF ($r = 0.51$, $p = 0.04$) and LVEDV ($r = -0.58$, $p = 0.02$). Delta R1 of IC showed a trend towards correlation with LVEF ($r = 0.50$, $p = 0.05$). On the other hand, native T1 of TI, IC, PIR, and RM did not show any correlation with LVEF, LVEDV, LVEDVI, LVM, or LVMI (Fig. 2).

To further confirm these relationships, the swine were divided into the higher EF group ($n = 8$) and the lower EF group ($n = 7$) by the median LVEF (28.9%) of 15 swine (Table 1). %Total infarct was significantly larger in the lower EF group compared to the higher EF group (33.9 ± 5.5% vs. 27.0 ± 5.0%, $p = 0.02$). %PIR showed an increased trend in the lower EF group (11.4 ± 6.8% vs. 5.7 ± 3.8%, $p = 0.08$) while the %IC was comparable in both groups (21.3% ± 4.9% vs. 22.5 ± 6.7%, $p = 0.69$) PIR mass was significantly increased in the lower EF group (7.7 ± 4.4 g) compared to the higher EF group (3.4 ± 2.1 g, $p = 0.02$) while the IC mass was comparable in both groups (15.7 ± 6.2 g (lower) vs. 13.6 ± 4.7 g (higher)). On the other hand, post-MEMRI T1 of PIR demonstrated significant reduction in the higher vs. lower EF group (1082.9 ± 98.6 ms vs. 1197.3 ± 60.7 ms, $p = 0.01$). However, post-MEMRI T1 of IC or RM did not have significant difference between the lower and higher EF groups (Table 1). Furthermore, delta R1 showed higher manganese uptake of PIR in the higher vs. lower EF group (0.270 ± 0.095 s^{-1} vs. 0.187 ± 0.029 s^{-1}, $p = 0.04$). Delta R1 of IC and RM also showed a trend towards higher manganese uptake in the higher EF group. In contrast, native T1 values of IC, PIR and RM could not be distinguished between the two groups.

These results suggested the lower myocardial viability signal of PIR as measured by post-MEMRI T1 and delta R1 are more strongly associated with LV dysfunction compared to IC and RM regions. Native T1 of any territory does not associate or correlate with any parameter of LV dysfunction.

Table 1
Native T1, post MEMRI T1, and delta R1, comparison between the higher EF and lower EF groups.

Native T1, post-MEMRI T1, and delta R1 values in each territory are described in the table.

	Native T1 (ms)	Post-MEMRI T1 (ms)	Delta R1 (s^{-1})	Size (% of LV)
TI	1615.9 ± 93.8	1235.8 ± 114.8	0.195 ± 0.089	30.2 ± 6.2
IC	1634.7 ± 88.4	1262.6 ± 126.8	0.186 ± 0.095	21.8 ± 5.6
PIR	1530.5 ± 75.2	1136.3 ± 99.6	0.231 ± 0.082	8.4 ± 5.9
RM	1406.4 ± 37.9	956.7 ± 138.1	0.359 ± 0.195	
Control (septum)	1406.8 ± 31.0	929.4 ± 159.6	0.387 ± 0.169	
Control (lateral)	1412.6 ± 89.1	965.0 ± 181.8	0.356 ± 0.199	

(MEMRI = manganese-enhanced MRI, TI = total infarct, IC = infarct core, PIR = peri-infarct region, RM = remote myocardium)

Data of higher EF group and lower EF group was compared. (p; higher EF vs lower EF, *$p < 0.05$)

		Higher EF ($n = 8$)	Lower EF ($n = 7$)	p
IC	Size (%LV)	21.3 ± 4.9	22.5 ± 6.7	0.69
	Size (g)	13.6 ± 4.7	15.7 ± 6.2	0.53
	Native T1 (ms)	1653.1 ± 96.8	1613.6 ± 79.5	0.4
	Post-MEMRI T1 (ms)	1221.6 ± 149.0	1309.5 ± 82.6	0.3
	Delta R1 (s^{-1})	0.222 ± 0.119	0.145 ± 0.028	0.11
PIR	Size (%LV)	5.7 ± 3.8	11.4 ± 6.8	0.08
	Size (g)	3.4 ± 2.1	7.7 ± 4.4	0.02*
	Native T1 (ms)	1519.1 ± 82.0	1543.5 ± 70.6	0.54
	Post-MEMRI T1 (ms)	1082.9 ± 98.6	1197.3 ± 60.7	0.01*
	Delta R1 (s^{-1})	0.270 ± 0.095	0.187 ± 0.029	0.04*
TI	Size (%LV)	27.0 ± 5.0	33.9 ± 5.5	0.02*
	Size (g)	17.1 ± 4.3	23.5 ± 5.9	0.04*
	Native T1 (ms)	1633.4 ± 109.6	1595.9 ± 75.1	0.44
	Post-MEMRI T1 (ms)	1198.2 ± 131.7	1278.7 ± 80.5	0.17
	Delta R1 (s^{-1})	0.229 ± 0.111	0.156 ± 0.029	0.11
RM	Native T1 (ms)	1404.5 ± 44.8	1408.6 ± 31.7	0.83
	Post-MEMRI T1 (ms)	908.4 ± 159.0	1012.0 ± 91.2	0.14
	Delta R1 (s^{-1})	0.423 ± 0.242	0.285 ± 0.095	0.17
LVEF	(%)	34.7 ± 5.9	20.0 ± 2.1	0.0001*
LVEDV	(ml)	67.1 ± 11.3	90.8 ± 14.2	0.004*
LVEDVI	(ml/m^2)	81.0 ± 19.9	109.5 ± 22.0	0.02*
LVM	(g)	63.0 ± 10.3	68.8 ± 11.5	0.33
LVMI	(g/m^2)	75.1 ± 13.4	82.9 ± 17.7	0.36
HR	(/min)	94.3 ± 25.2	94.7 ± 10.6	0.97

(IC = infarct core, PIR = peri-infarct region, TI = total infarct, RM = remote myocardium, LVEDV = LV end-diastolic volume, LVEDVI = LVEDV index, LVM = LV mass, LVMI = LVM index, HR = heart rate, MEMRI = manganese-enhanced MRI).

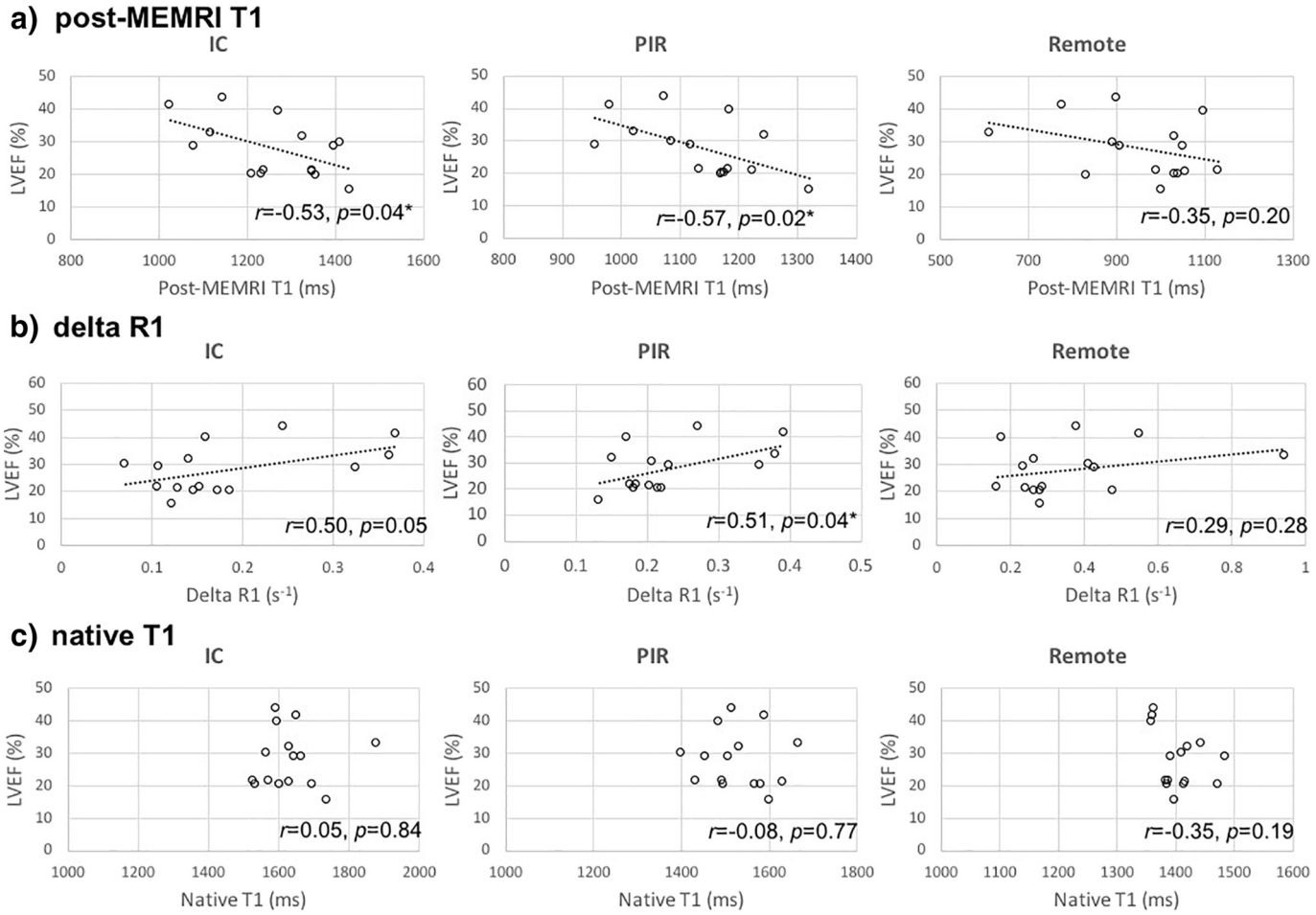

Fig. 2. Correlation of Native T1, post-MEMRI T1, and delta R1 with cardiac function. Correlations of post-MEMRI T1 values (a), delta R1 (b), and native T1 values (c) with LVEF are shown the graphs (*$p < 0.05$).

3.3. MEMRI and arrhythmogenicity

Ten swine underwent electrophysiological study (EPS) for inducibility of ventricular arrhythmia. Total infarct volume significantly correlated with arrhythmogenicity indicated by shorter baseline-S2 interval ($r = -0.68$, $p = 0.003$) where negative correlation (i.e. longer cycle length to induce arrhythmia) shows higher arrhythmogenicity. Native T1 or post-MEMRI T1 did not show significant correlation with arrhythmogenesis. However, delta R1, representing the differential manganese uptake, demonstrated a trend towards correlation of the following regions of myocardial injury with arrhythmogenicity: IC ($r = -0.27$, $p = 0.43$), PIR ($r = -0.32$, $p = 0.36$), and RM ($r = -0.53$, $p = 0.10$) as illustrated in Fig. 3. The region with higher myocardial manganese uptake appears to be more susceptible to LV arrhythmia.

3.4. Histological evaluation of the infarct zones

The cross sectional slice of the excised heart was compared with the MRI finding. Inside the Evans blue negative AAR, TTC negative IC and TTC positive PIR were confirmed (Supplementary Fig. 2a–b). The distribution of IC and PIR corresponded well with MRI findings. H&E staining confirmed TTC negative IC was composed of necrosis and fibrosis (Supplementary Fig. 2c) and PIR contained mixed components of cardiomyocyte, fibrosis and infiltration of inflammatory cells (Supplementary Fig. 2d). The remote myocardium did not show abnormal findings (Supplementary Fig. 2e).

4. Discussion

4.1. Major findings of this study

In this study, we segmented the post IR myocardial injury into 3 territories (IC, PIR and RM) and demonstrated distinct native T1 and manganese uptake properties of these territories. Mean MEMRI signal of PIR correlated significantly with LV function. This finding suggested the myocardial viability of PIR may underlie the progressive LV remodeling compared to IC or RM. Native T1 lacked sufficient contrast to exhibit correlation with LV function. This study found a trend towards LV arrhythmia inducibility with higher myocardial manganese uptake of each territory.

4.2. PIR characterization by MEMRI

There has been no consistent method to quantify the degree of mixed cellular composition and injured cardiomyocytes in the PIR. The present study successfully differentiated and measured the PIR viability based on the myocardial manganese uptake. The intermediate native and post-MEMRI T1 of PIR is suggestive of its heterogeneous tissue composition, consisting of injured cardiomyocytes and fibrosis.

Although the importance of PIR as an independent predictor of major adverse clinical events has been noted recently, the quantification of PIR by post-MEMRI T1 mapping has not been reported [4,11,28,29]. In this study, quantitative MEMRI measurement of PIR viability showed significant correlation with LV function. Our results indicate the post-MEMRI T1 correlate strongly with LVEF while delta R1 may

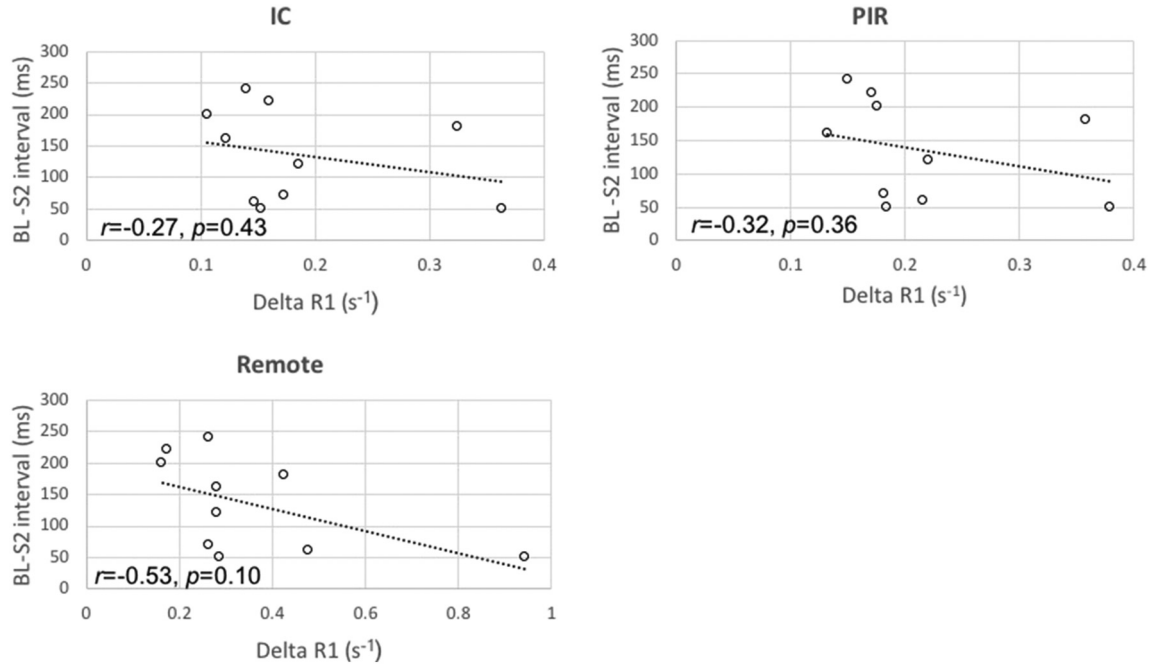

Fig. 3. Arrhythmogenesis and delta R1 in IC, PIR, and Remote. The EPS data are plotted against the delta R1 (myocardial manganese uptake) of IC, PIR, and Remote. Shorter BL-S2 interval means higher inducibility of ventricular arrhythmia.

quantify myocardial viability more accurately and provide clinically relevant data.

Recent studies have revealed PIR represents the nexus for active remodeling characterized by extracellular matrix formation, angiogenesis, oxidative stress, mitochondrial energetics, apoptosis and inflammation [9,30–32]. Those active and dynamic reactions could lead to its heterogeneity and arrhythmogenic substrates. The exact reason why higher myocardial manganese uptake (delta R1) of each region correlated with arrhythmogenesis in this study remains unknown; however, MEMRI signal could also correlate with the electrophysiological stability of the cardiomyocytes, indicating LV arrhythmogenic potential. Our results lend insight into the outcomes of clinical trials showing that LVEF alone is an insufficient marker to select patients for ICD implantation [15,33]. Further study will be necessary to confirm this relationship.

Diagnostic values of native T1 and ECV in acute myocardial infarction in predicting LV dysfunction have been reported in several clinical studies [16–18,34]. However, native T1 did not correlate with LV function subacutely with the limited sample size in this study. Extracellular volume (ECV) evaluation by DEMRI and MEMRI viability analysis assesses different aspects of myocardial injury, i.e. alterations in the interstitium and cardiomyocytes [35]. In this study, ECV analysis could not be performed reliably due to interference from the residual intracellular signal of manganese. In the future, unique strengths of each contrast agent must be leveraged to better delineate the role of the PIR in HF.

In this study, a 4-week time point after IR was adopted to evaluate the ongoing remodeling process post IR injury. Patients with LV dysfunction following myocardial infarction have a markedly increased 6-month mortality and the incidence of sudden cardiac death is increased especially during the first month post-MI [33,36,37]. This intermediate time point may be important in clinical management plan regarding revascularization, implantable cardioverter defibrillator (ICD) implantation, or novel therapeutics. However, further studies to characterize the PIR at different time points are required to investigate the prognostic importance and the underlying mechanisms of the IR injury resulting in LV remodeling and arrhythmogenesis.

4.3. Safety of MEMRI

The clinical relevance and safety profile is evidenced by the FDA Investigational New Drug approval status of our clinical trial to employ the contrast agent, EVP1001-1, to study severe ischemic cardiomyopathy patients. This study is on-going in our Lab currently. Manganese-based contrast agent could cause adverse cardiovascular side effects including negative inotropic effect and hypotension at high concentration. Most studies to date have used 5 to 30 μmol/kg Mn^{2+} concentration, which eliminated serious toxicities. The unique formulation of EVP1001-1 and manganese dose within this known concentration range enables high safety profile [20,38].

4.4. Myocardial T1 mapping using SMART1Mmap sequence

T1mapping in this study was obtained using SMART1Map sequence, which employs a single-point, saturation-recovery acquisition [26]. Saturation recovery method allows the highest agreement with the gold standard inversion recovery spin echo T1 mapping; which gives a higher native T1 value of the myocardium by 300 ms compared to Look-Locker based method such as MOLLI or ShMOLLI [39]. T1 values are field strength dependent, generating higher values at 3 T compared to 1.5 T [40]. This may explain the higher T1 values obtained in this study compared to other studies, which employ MOLLI or ShMOLLI sequences.

4.5. Limitations

The analysis performed in this study used images obtained at the identical image prescription and cardiac phase. However, different heart rate at the time of scan and possible mis-registration of slices on MRI sequences could cause displacement of the injured myocardium and inconsistent calculation of T1 values. Furthermore, the border area between IC and PIR could be affected by partial volume effect. However, any image processing was avoided to eliminate the risk of losing the unique characteristics of PIR. Our 4SD method to delineate infarct has not been validated histologically. Although multiple methods have

been proposed to quantitate the infarct signal, 4SD is reported to have a good agreement with the manual threshold and a strong correlation with a biomarker-based assessment of myocardial injury [41]. Recent studies have shown the agreement between DEMRI and post contrast T1 mapping in determining the infarct size [42,43]. However, this method has not been widely used. In addition, T1 mapping by saturation recovery method, which is known to be more accurate but less precise, has never been applied for delineating infarct [44]. In this study, we adopted a well-established infarct segmentation method [45]. Our results showed overlap of T1 values between IC and PIR, which suggests infarct segmentations based on delayed enhancement may not correspond with those on T1 mapping.

The analysis in this study could not prove the strongest correlation of PIR with LV dysfunction compared to that of IC or RM. The current study was also limited to a single timepoint. We plan to conduct a serial analysis to evaluate the temporal relationship of the PIR to the overall development of LV dysfunction, remodeling and arrhythmia. A larger sample size will be necessary to confirm these pathophysiologic relationships.

5. Conclusion

Precise characterization of myocardial viability in IC, PIR, and RM is feasible using T1 mapping post-MEMRI. Cardiac viability of PIR quantified specifically by post-MEMRI T1 mapping correlates with cardiac dysfunction.

Supplementary data to this article can be found online at https://doi.org/10.1016/j.ijcard.2019.01.101.

Sources of funding

NIH 5UM1 (PCY, USA). General Electric Healthcare (PCY, USA). California Institute for Regenerative Medicine RT3-07798 and DR2A-05394 (JCW, USA). NIH R01 HL133271 (JCW, USA). Japanese Circulation Society (YT, Japan). Fulbright Commission (JZ, UK). British Heart Foundation (JZ, UK).

Disclosures

This research did not receive any specific grant from funding agencies in the public, commercial, or not-for-profit sectors.

Conflict of interest

The authors report no relationships that could be construed as a conflict of interest.

Acknowledgement

None.

References

[1] G. Heusch, P. Libby, B. Gersh, D. Yellon, M. Böhm, G. Lopaschuk, et al., Cardiovascular remodelling in coronary artery disease and heart failure, Lancet 383 (2014) 1933–1943.
[2] M. Tsukiji, P. Nguyen, G. Narayan, J. Hellinger, F. Chan, R. Herfkens, et al., Peri-infarct ischemia determined by cardiovascular magnetic resonance evaluation of myocardial viability and stress perfusion predicts future cardiovascular events in patients with severe ischemic cardiomyopathy, J. Cardiovasc. Magn. Reson. 8 (2006) 773–779.
[3] H. Yokota, S. Heidary, C.K. Katikireddy, P. Nguyen, J.M. Pauly, M.V. McConnell, et al., Quantitative characterization of myocardial infarction by cardiovascular magnetic resonance predicts future cardiovascular events in patients with ischemic cardiomyopathy, J. Cardiovasc. Magn. Reson. 10 (2008) 17.
[4] S. Heidary, H. Patel, J. Chung, H. Yokota, S.N. Gupta, M.V. Bennett, et al., Quantitative tissue characterization of infarct core and border zone in patients with ischemic cardiomyopathy by magnetic resonance is associated with future cardiovascular events, J. Am. Coll. Cardiol. 55 (2010) 2762–2768.
[5] R.M. Judd, C.H. Lugo-Olivieri, M. Arai, T. Kondo, P. Croisille, J.A. Lima, et al., Physiological basis of myocardial contrast enhancement in fast magnetic resonance images of 2-day-old reperfused canine infarcts, Circulation 92 (1995) 1902–1910.
[6] M. Saeed, J. Bremerich, M.F. Wendland, R. Wyttenbach, H.J. Weinmann, C.B. Higgins, Reperfused myocardial infarction as seen with use of necrosis-specific versus standard extracellular MR contrast media in rats, Radiology 213 (1999) 247–257.
[7] M. Saeed, G. Lund, M.F. Wendland, J. Bremerich, H. Weinmann, C.B. Higgins, Magnetic resonance characterization of the peri-infarction zone of reperfused myocardial infarction with necrosis-specific and extracellular nonspecific contrast media, Circulation 103 (2001) 871–876.
[8] H. Arheden, M. Saeed, C.B. Higgins, D.W. Gao, P.C. Ursell, J. Bremerich, et al., Reperfused rat myocardium subjected to various durations of ischemia: estimation of the distribution volume of contrast material with echo-planar MR imaging, Radiology 215 (2000) 520–528.
[9] J.M. Duran, S. Taghavi, R.M. Berretta, C.A. Makarewich, T. Sharp Iii, T. Starosta, et al., A characterization and targeting of the infarct border zone in a swine model of myocardial infarction, Clin. Transl. Sci. 5 (2012) 416–421.
[10] A. Schmidt, C.F. Azevedo, A. Cheng, S.N. Gupta, D.A. Bluemke, T.K. Foo, et al., Infarct tissue heterogeneity by magnetic resonance imaging identifies enhanced cardiac arrhythmia susceptibility in patients with left ventricular dysfunction, Circulation 115 (2007) 2006–2014.
[11] A.T. Yan, A.J. Shayne, K.A. Brown, S.N. Gupta, C.W. Chan, T.M. Luu, et al., Characterization of the peri-infarct zone by contrast-enhanced cardiac magnetic resonance imaging is a powerful predictor of post-myocardial infarction mortality, Circulation 114 (2006) 32–39.
[12] T.C. Hung, Y. Suzuki, T. Urashima, A. Caffarelli, G. Hoyt, A.Y. Sheikh, et al., Multimodality evaluation of the viability of stem cells delivered into different zones of myocardial infarction, Circ. Cardiovasc. Imaging 1 (2008) 6–13.
[13] P.K. Nguyen, F. Lan, Y. Wang, J.C. Wu, Imaging: guiding the clinical translation of cardiac stem cell therapy, Circ. Res. 109 (2011) 962–979.
[14] E. Golcuk, K. Yalin, T. Aksu, S.K. Tiryakioglu, A.K. Bilge, K. Adalet, Peri-infarction zone as a risk marker for patients with postmyocardial infarction, Am J Med Sci 351 (2016) 452–458.
[15] S.D. Roes, C.J. Borleffs, R.J. van der Geest, J.J. Westenberg, N.A. Marsan, T.A. Kaandorp, et al., Infarct tissue heterogeneity assessed with contrast-enhanced MRI predicts spontaneous ventricular arrhythmia in patients with ischemic cardiomyopathy and implantable cardioverter-defibrillator, Circ. Cardiovasc. Imaging 2 (2009) 183–190.
[16] M. Ugander, A.J. Oki, L.Y. Hsu, P. Kellman, A. Greiser, A.H. Aletras, et al., Extracellular volume imaging by magnetic resonance imaging provides insights into overt and sub-clinical myocardial pathology, Eur. Heart J. 33 (2012) 1268–1278.
[17] J. Carberry, D. Carrick, C. Haig, S.M. Rauhalammi, N. Ahmed, I. Mordi, et al., Remote zone extracellular volume and left ventricular remodeling in survivors of ST-elevation myocardial infarction, Hypertension 68 (2016) 385–391.
[18] A. Kidambi, M. Motwani, A. Uddin, D.P. Ripley, A.K. McDiarmid, P.P. Swoboda, et al., Myocardial extracellular volume estimation by CMR predicts functional recovery following acute MI, JACC Cardiovasc. Imaging 10 (2017) 989–999.
[19] G.A. Krombach, M. Saeed, C.B. Higgins, V. Novikov, M.F. Wendland, Contrast-enhanced MR delineation of stunned myocardium with administration of MnCl (2) in rats, Radiology 230 (2004) 183–190.
[20] M.F. Wendland, Applications of manganese-enhanced magnetic resonance imaging (MEMRI) to imaging of the heart, NMR Biomed. 17 (2004) 581–594.
[21] R. Dash, J. Chung, F. Ikeno, A. Hahn-Windgassen, Y. Matsuura, M.V. Bennett, et al., Dual manganese-enhanced and delayed gadolinium-enhanced MRI detects myocardial border zone injury in a pig ischemia-reperfusion model, Circ. Cardiovasc. Imaging 4 (2011) 574–582.
[22] R. Dash, P.J. Kim, Y. Matsuura, F. Ikeno, S. Metzler, N.F. Huang, et al., Manganese-enhanced magnetic resonance imaging enables in vivo confirmation of peri-infarct restoration following stem cell therapy in a porcine ischemia-reperfusion model, J. Am. Heart Assoc. 4 (2015).
[23] P. Storey, P.G. Danias, M. Post, W. Li, P.R. Seoane, P.P. Harnish, et al., Preliminary evaluation of EVP 1001-1: a new cardiac-specific magnetic resonance contrast agent with kinetics suitable for steady-state imaging of the ischemic heart, Investig. Radiol. 38 (2003) 642–652.
[24] R. Eriksson, L. Johansson, T. Bjerner, H. Ahlström, Dobutamine-induced stress affects intracellular uptake of manganese: a quantitative magnetic resonance imaging study in pigs, J. Magn. Reson. Imaging 21 (2005) 360–364.
[25] S. Flacke, J.S. Allen, J.M. Chia, J.H. Wible, M.P. Periasamy, M.D. Adams, et al., Characterization of viable and nonviable myocardium at MR imaging: comparison of gadolinium-based extracellular and blood pool contrast materials versus manganese-based contrast materials in a rat myocardial infarction model, Radiology 226 (2003) 731–738.
[26] Stainsby Sa, True T1 mapping with SMART 1 Map (saturation method using adaptive recovery times for cardiac T 1 mapping): a comparison with MOLLI, J. Cardiovasc. Magn. Reson. (2013) 3.
[27] K.W. Kelley, S.E. Curtis, G.T. Marzan, H.M. Karara, C.R. Anderson, Body surface area of female swine, J. Anim. Sci. 36 (1973) 927–930.
[28] E. Watanabe, S.A. Abbasi, B. Heydari, O.R. Coelho-Filho, R. Shah, T.G. Neilan, et al., Infarct tissue heterogeneity by contrast-enhanced magnetic resonance imaging is a novel predictor of mortality in patients with chronic coronary artery disease and left ventricular dysfunction, Circ. Cardiovasc. Imaging 7 (2014) 887–894.
[29] J. Ringenberg, M. Deo, D. Filgueiras-Rama, G. Pizarro, B. Ibañez, R. Peinado, et al., Effects of fibrosis morphology on reentrant ventricular tachycardia inducibility and simulation fidelity in patient-derived models, Clin. Med. Insights Cardiol. 8 (2014) 1–13.
[30] L. Yang, Z.R. Gregorich, W. Cai, P. Zhang, B. Young, Y. Gu, et al., Quantitative proteomics and immunohistochemistry reveal insights into cellular and molecular processes

in the infarct border zone one month after myocardial infarction, J. Proteome Res. 16 (2017) 2101–2112.
[31] I. Roifman, N.R. Ghugre, T. Vira, M.I. Zia, A. Zavodni, M. Pop, et al., Assessment of the longitudinal changes in infarct heterogeneity post myocardial infarction, BMC Cardiovasc. Disord. 16 (2016) 198.
[32] R. Fernández-Jiménez, J. García-Prieto, J. Sánchez-González, J. Agüero, G.J. López-Martín, C. Galán-Arriola, et al., Pathophysiology underlying the bimodal edema phenomenon after myocardial ischemia/reperfusion, J. Am. Coll. Cardiol. 66 (2015) 816–828.
[33] C.S. Elayi, R.J. Charnigo, P.M. Heron, B.K. Lee, J.E. Olgin, Primary prevention of sudden cardiac death early post-myocardial infarction: root cause analysis for implantable cardioverter-defibrillator failure and currently available options, Circ. Arrhythm. Electrophysiol. 10 (2017).
[34] D. Liu, A. Borlotti, D. Viliani, M. Jerosch-Herold, M. Alkhalil, G.L. De Maria, et al., CMR native T1 mapping allows differentiation of reversible versus irreversible myocardial damage in ST-segment-elevation myocardial infarction: an OxAMI study (Oxford Acute Myocardial Infarction), Circ. Cardiovasc. Imaging 10 (2017).
[35] J.C. Moon, D.R. Messroghli, P. Kellman, S.K. Piechnik, M.D. Robson, M. Ugander, et al., Myocardial T1 mapping and extracellular volume quantification: a Society for Cardiovascular Magnetic Resonance (SCMR) and CMR Working Group of the European Society of Cardiology consensus statement, J. Cardiovasc. Magn. Reson. 15 (2013) 92.
[36] R.J. Burns, R.J. Gibbons, Q. Yi, R.S. Roberts, T.D. Miller, G.L. Schaer, et al., The relationships of left ventricular ejection fraction, end-systolic volume index and infarct size to six-month mortality after hospital discharge following myocardial infarction treated by thrombolysis, J. Am. Coll. Cardiol. 39 (2002) 30–36.
[37] E. Puymirat, T. Simon, G. Cayla, Y. Cottin, M. Elbaz, P. Coste, et al., Acute myocardial infarction: changes in patient characteristics, management, and 6-month outcomes over a period of 20 years in the FAST-MI Program (French Registry of Acute ST-Elevation or Non-ST-elevation Myocardial Infarction) 1995 to 2015, Circulation 136 (2017) 1908–1919.
[38] J.L. Fernandes, P. Storey, J.A. da Silva, G.S. de Figueiredo, J.M. Kalaf, O.R. Coelho, Preliminary assessment of cardiac short term safety and efficacy of manganese chloride for cardiovascular magnetic resonance in humans, J. Cardiovasc. Magn. Reson. 13 (2011) 6.
[39] T. Teixeira, T. Hafyane, N. Stikov, C. Akdeniz, A. Greiser, M.G. Friedrich, Comparison of different cardiovascular magnetic resonance sequences for native myocardial T1 mapping at 3 T, J. Cardiovasc. Magn. Reson. 18 (2016) 65.
[40] D. Dabir, N. Child, A. Kalra, T. Rogers, R. Gebker, A. Jabbour, et al., Reference values for healthy human myocardium using a T1 mapping methodology: results from the International T1 Multicenter cardiovascular magnetic resonance study, J. Cardiovasc. Magn. Reson. 16 (2014) 69.
[41] B.T. Costello, D. Stub, J. Hare, A.H. Ellims, X. Wang, K. Smith, et al., Comparison of magnetic resonance analysis of myocardial scarring with biomarker release following S-T elevation myocardial infarction, Heart Lung Circ. (2018) pii: S1443-9506 (18) 30070-2.
[42] H. Bulluck, M. Hammond-Haley, M. Fontana, D.S. Knight, A. Sirker, A.S. Herrey, et al., Quantification of both the area-at-risk and acute myocardial infarct size in ST-segment elevation myocardial infarction using T1-mapping, J. Cardiovasc. Magn. Reson. 19 (2017) 57.
[43] P. Garg, D.A. Broadbent, P.P. Swoboda, J.R.J. Foley, G.J. Fent, T.A. Musa, et al., Acute infarct extracellular volume mapping to quantify myocardial area at risk and chronic infarct size on cardiovascular magnetic resonance imaging, Circ. Cardiovasc. Imaging 10 (2017).
[44] P. Kellman, M.S. Hansen, T1-mapping in the heart: accuracy and precision, J. Cardiovasc. Magn. Reson. 16 (2014) 2.
[45] J. Schulz-Menger, D.A. Bluemke, J. Bremerich, S.D. Flamm, M.A. Fogel, M.G. Friedrich, et al., Standardized image interpretation and post processing in cardiovascular magnetic resonance: Society for Cardiovascular Magnetic Resonance (SCMR) board of trustees task force on standardized post processing, J. Cardiovasc. Magn. Reson. 15 (2013) 35.